Supporting Information

Repurposing of Four Drugs as Anti-SARS-CoV-2 Agents and Their Interactions with Protein Targets

Luis C. Vesga [1], Camilo A. Ruiz-Hernández [1], Jeimmy J. Alvarez-Jácome [1], Jonny E. Duque [2], Bladimiro Rincón-Orozco [1,3], Stelia Carolina Mendez-Sanchez [1,3,*]

[1] Grupo de Investigación en Bioquímica y Microbiología (GIBIM), Universidad Industrial de Santander A. A. 678, Piedecuesta 681027, Colombia; luis.vesga@correo.uis.edu.co (L.C.V.); camilo2162151@correo.uis.edu.co (C.A.R.-H.); jeimmy2171468@correo.uis.edu.co (J.J.A.-J.); blrincon@uis.edu.co (B.R.-O.)

[2] Centro de Investigación en Enfermedades Tropicales (CINTROP), Universidad Industrial de Santander A. A. 678, Piedecuesta 681027, Colombia; jonedulu@uis.edu.co

[3] Grupo de Investigación en Compuestos Orgánicos de Interés Medicinal CODEIM, Universidad Industrial de Santander A. A. 678, Piedecuesta 681027, Colombia

* Corresponding author: scmendez@uis.edu.co

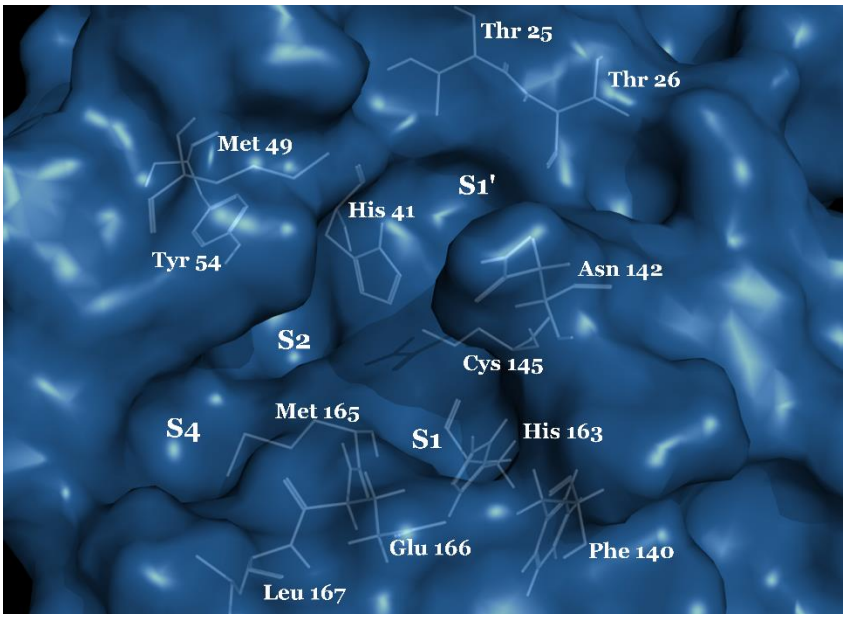

Figure S1. Surface representation of substrate-binding pocket in SARS-CoV-2 M^{pro}. Relevant amino acid residues, S1, S1', S2, and S4 subsites are indicated. Figure adapted of Jin et al., 2020 [1].

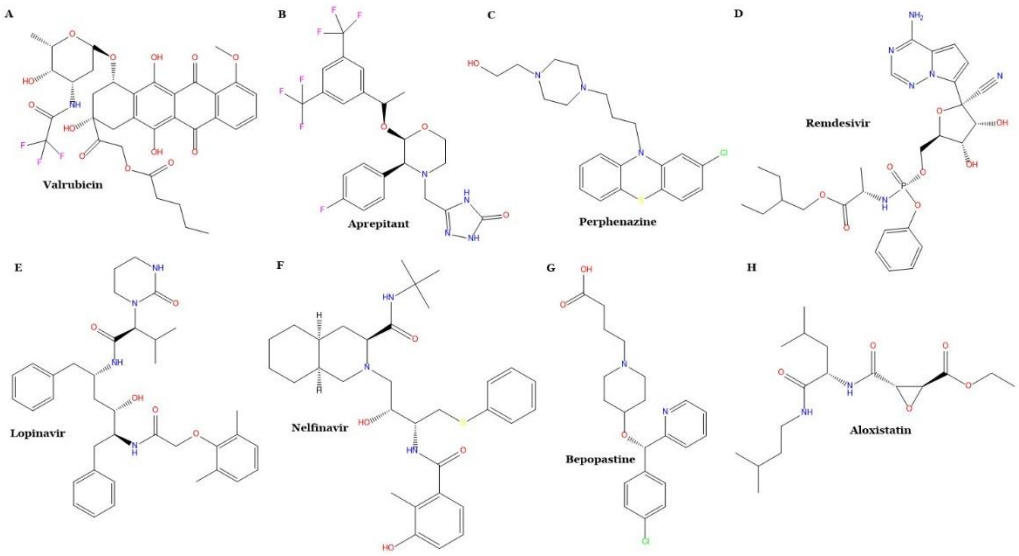

Figure S2. List of principal drugs previously predicted as M^{pro} inhibitors: (**A**) Valrubicin, (**B**) Aprepitant, (**C**) Perphenazine, (**D**) Remdesivir, (**E**) Lopinavir, (**F**) Nelfinavir, (**G**) Bepopastine, (**H**) Aloxistatin.

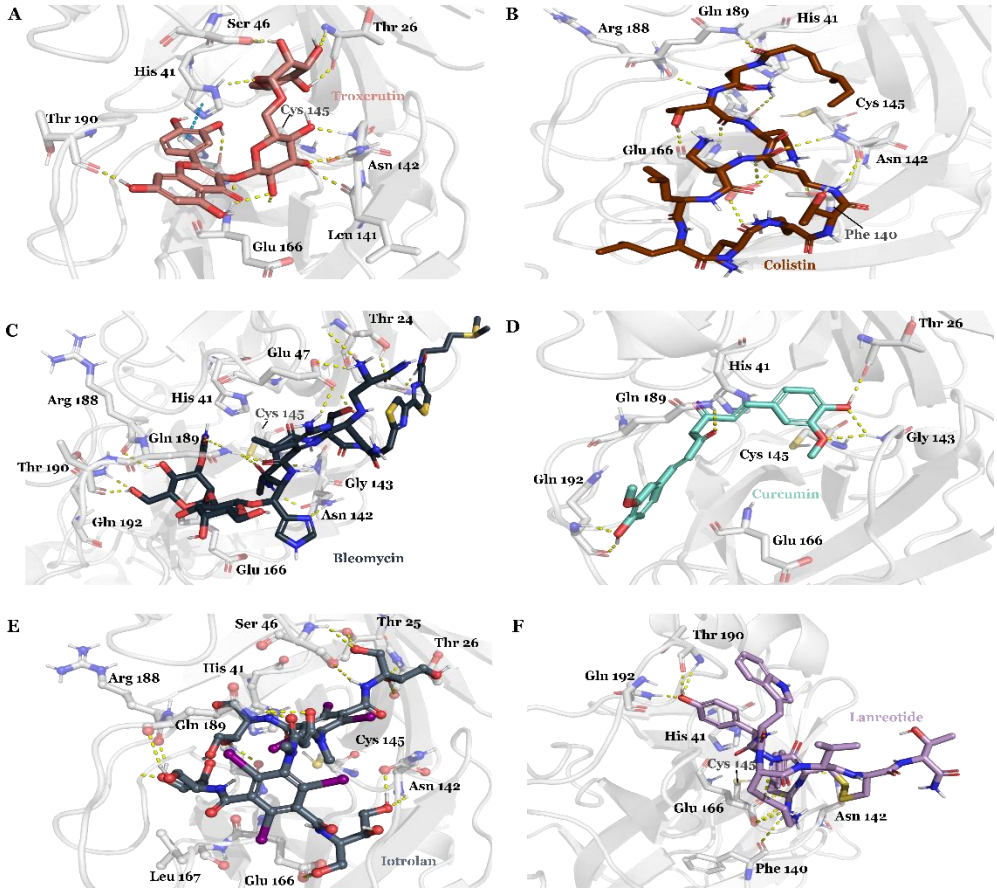

Figure S3. Representative snapshots of the docking pose of best ranked FDA-approved drugs interacting in M^{pro}. Suggested possible orientations of troxerutin (**A**), colistin (**B**), bleomycin (**C**), curcumin (**D**), Iotrolan (**E**), lanreotide (**F**). M^{pro}'s residues are colored according to the atom type of the interacting amino-acid residues (protein's carbon, light grey; oxygen, red; nitrogen, blue). The protein-ligand interactions are represented by dash lines as follow: hydrogen bond interactions are colored in yellow, and π-π interactions are colored in blue.

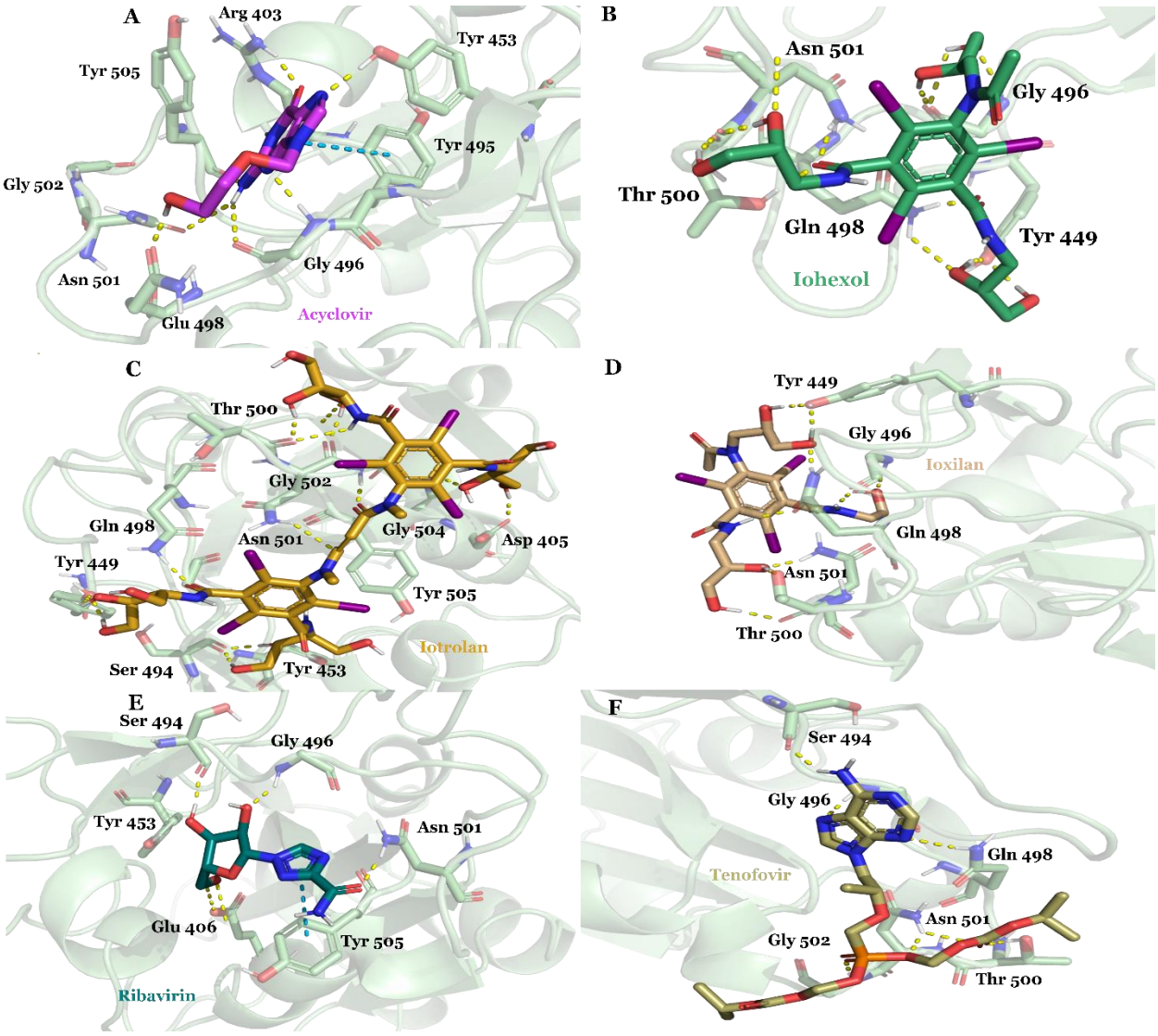

Figure S4. Representative snapshots of the docking poses of best ranked FDA-approved drug in S protein. Suggested possible orientations of acyclovir (**A**), iohexol (**B**), iotrolan (**C**), ioxilan (**D**), ribavirin (**E**), tenofovir (**F**). S-protein's residues are colored according to the atom type of the interacting amino-acid residues (protein's

carbon, pale green; oxygen, red; nitrogen, blue). The protein-ligand interactions are represented by dash lines as follow: hydrogen bond interactions are colored in yellow, and π-π interactions are colored in blue.

Table S1. Docking score and free binding energy calculation of best 15 ranked FDA-approved drugs against SARS-CoV-2 Spike glycoprotein (S-protein) B.1.1.7 (Alpha) variant.

Compound ID	Traditional Name	FDA Status	Docking Score	$\Delta G_{(bind)}$ $kcal/mol$	Biological Activity
DB09059	Atosiban	Approved	-5,204	-66.43	Oxytocin receptor [2]
DB04703	Hesperidin	Approved,	-6,284	-64,44	Anti-cancer effect [3]
DB00183	Pentagastrin	Approved	-6,680	-62,36	Gastrin/cholecystokinin type B receptor [4]
DB06814	Protokylol	Approved,	-5,577	-57,85	Protein homodimerization [5]
DB08947	Iopamidol	Approved	-6,535	-52,36	Contrast agent [6]
DB09313	Ioxaglic acid	Approved,	-5,487	-52,13	Contrast for X-Ray images [7]
DB00503	Ritonavir	Approved	-7,212	-50,93	HIV-1 inhibitor [8]
DB09142	Sincalide	Approved	-5,280	-49,16	Organic transmembrane transporter [9]
DB11705	Iomeprol	Approved,	-6,604	-48,31	Contrast agent [10]
DB09135	Ioxilan	Approved	-5,670	-46,29	Opacification of vessels in contrast médium [11]
DB03310	Glutathione disulfide	Approved,	-4,853	-45,29	Antitumor agent [12]
DB00650	Leucovorin	Approved	-4,804	-39,82	Drug antidote for folic acid antagonists [13] Cancer treatment [14]
DB09487	Iotrolan	Approved	-7,544	-38,04	Isotonic contrast medium for intrathecal use [15]
DB06441	Cangrelor	Approved	-5,388	-36,72	ADP and ATP receptor [16]
DB01362	Iohexol	Approved	-5,972	-34,43	Radiocontrast agent [17,18]

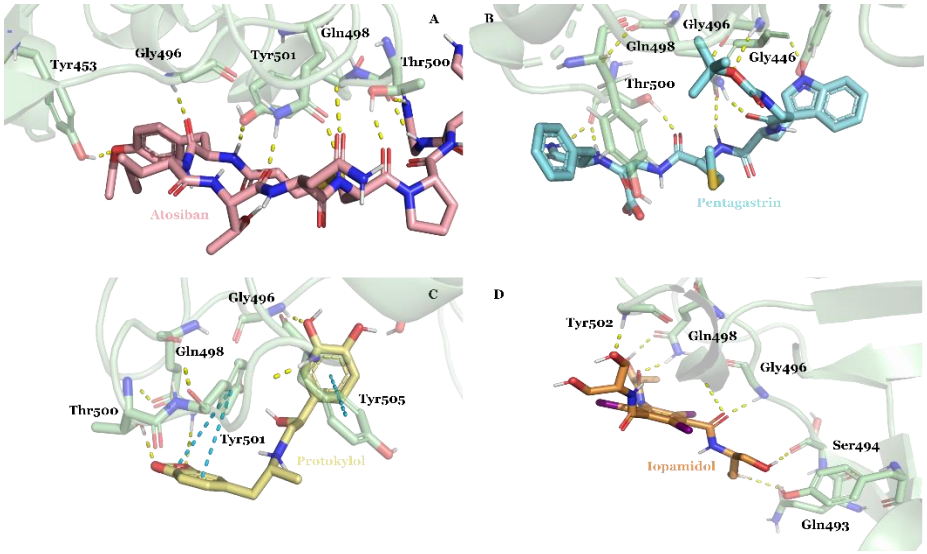

Figure S5. Representative snapshots of the docking poses of best ranked FDA-approved drug in B.1.1.7 (Alpha) variant. Suggested possible orientations of atosiban (**A**), pentagastrin (**B**), protkylol (**C**), iopamidol (**D**).S-protein's residues are colored according to the atom type of the interacting amino-acid residues (protein's carbon, pale green; oxygen, red; nitrogen, blue). The protein-ligand interactions are represented by dash lines as follow: hydrogen bond interactions are colored in yellow, and π-π interactions are colored in blue.

Table S2. Docking score and free binding energy calculation of best 15 ranked FDA-approved drugs against SARS-CoV-2 Spike glycoprotein (S-protein) B.1.351 (Beta) variant.

Compound ID	Traditional Name	FDA Status	Docking Score	$\Delta G_{(bind)}$ $kcal/mol$	Biological Activity
DB04703	Hesperidin	Approved,	-6,516	-65,70	Anti-cancer effect [3]
DB15494	Edotreotide gallium Ga-68	Approved	-6,810	-65,16	Somatostatin receptor types 1, 2, 3 and 5 [19]
DB01698	Rutin	Approved	-8,164	-61,76	Prostaglandin-e2 9-reductase activity [20]
DB09487	Iotrolan	Approved	-8,472	-59,28	Contrast agent [15]
DB09313	Ioxaglic acid	Approved	-6,043	-59,09	Contrast for X-Ray images [7]
DB06213	Regadenoson	Approved,	-5,654	-57,34	Identical protein binding. Adenosine receptor [21]
DB09134	Ioversol	Approved	-6,528	-53,66	Contrast dye for diagnosis procedures [22]
DB01249	Iodixanol	Approved	-10,181	-53,18	Radiocontrast agent [23]
DB00503	Ritonavir	Approved	-6,980	-50,15	HIV-1 inhibitor [8]
DB09142	Sincalide	Approved	-5,705	-47,59	Organic transmembrane transporter [9]
DB06791	Lanreotide	Approved	-5,663	-42,00	Anticancer [24]
DB15617	Ferric derisomaltose	Approved	-6,886	-40,66	Hemoglobin subunit Alpha [25] Transferrin receptor [26]
DB00183	Pentagastrin	Approved	-6,910	-37,81	Gastrin/cholecystokinin type B receptor [4]
DB09146	Iron sucrose	Approved	-7,775	-36,69	Iron anemia deficiency treatment [27]
DB01362	Iohexol	Approved	-8,606	-36,19	Radiocontrast agent [17,18]

Table S3. Docking score and free binding energy calculation of best 15 ranked FDA-approved drugs against SARS-CoV-2 Spike glycoprotein (S-protein) B.1.617.2 (Delta) variant.

Compound ID	Traditional Name	FDA Status	Docking Score	$\Delta G_{(bind)}$ *kcal/mol*	Biological Activity
DB00014	Goserelin	approved	-8.681	-41.75	Treat breast cancer [28], prostate cancer [29]
DB00284	Acarbose	approved	-7.874	-54.53	Antidiabetic [30,31]
DB00803	Colistin	approved	-7.613	-48.44	Antibiotic [32]
DB14642	Lypressin	approved	-6.981	-43.82	Treatment of diabetes insipidus [33]
DB03310	Glutathione disulfide	approved	-6.489	-12.99	Antitumor agent [12]
DB01362	Iohexol	approved	-6.326	-16.46	Radiocontrast agent [17,18]
DB06791	Lanreotide	approved	-6.097	-46.04	Anticancer [24]
DB01598	Imipenem	approved	-6.043	-17.56	Antibiotic [34]
DB00399	Zoledronic acid	approved	-5.653	-14.59	Treatment of osteoporosis [35], bone metastases, hypercalcemia of malignancy, multiple mieloma [36]
DB03147	Flavin adenine dinucleotide	approved	-5.679	-53.48	Treatment of hypertensive vascular remodeling [37]
DB00007	Leuprolide	approved	-5.596	-38.99	Anticancer [38,39]
DB01249	Iodixanol	approved	-5.330	-36.46	Radiocontrast agent [23]
DB09156	Iopromide	approved	-4.285	-49.48	X-ray contrast agent [40]

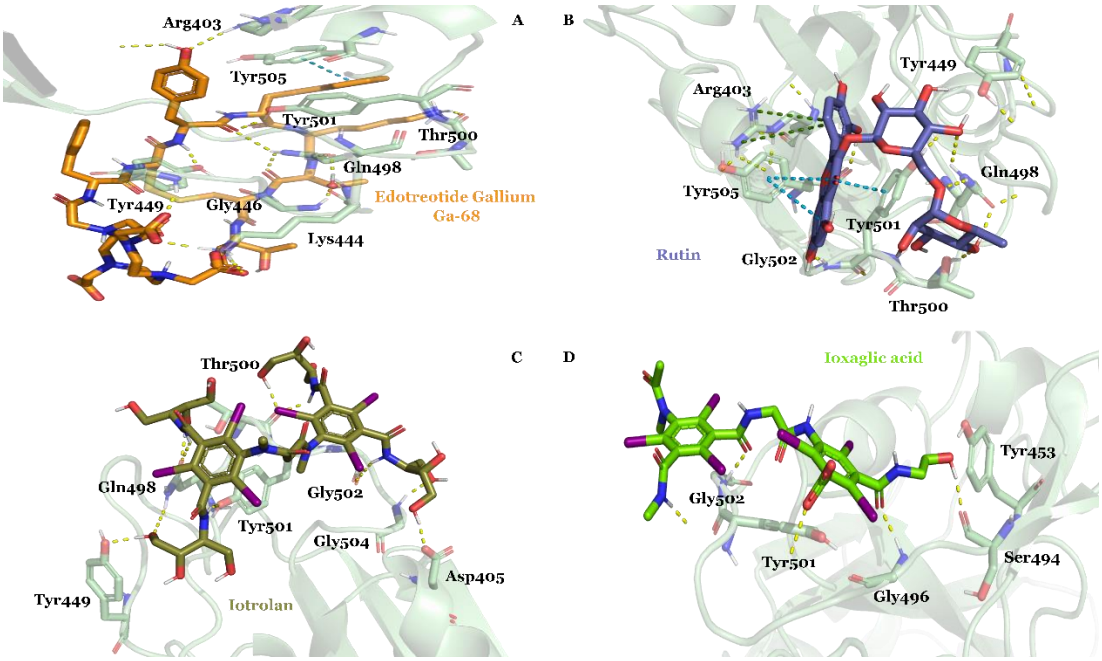

Figure S6. Representative snapshots of the docking poses of best ranked FDA-approved drug in B.1.351 (Beta) variant. Suggested possible orientations of Edotrotide Gallium (**A**), rutin (**B**), iotrolan (**C**), ioxaglic acid (**D**).S-protein's residues are colored according to the atom type of the interacting amino-acid residues (protein's carbon, pale green; oxygen, red; nitrogen, blue). The protein-ligand interactions are represented by dash lines as follow: hydrogen bond interactions are colored in yellow, and π-π interactions are colored in blue.

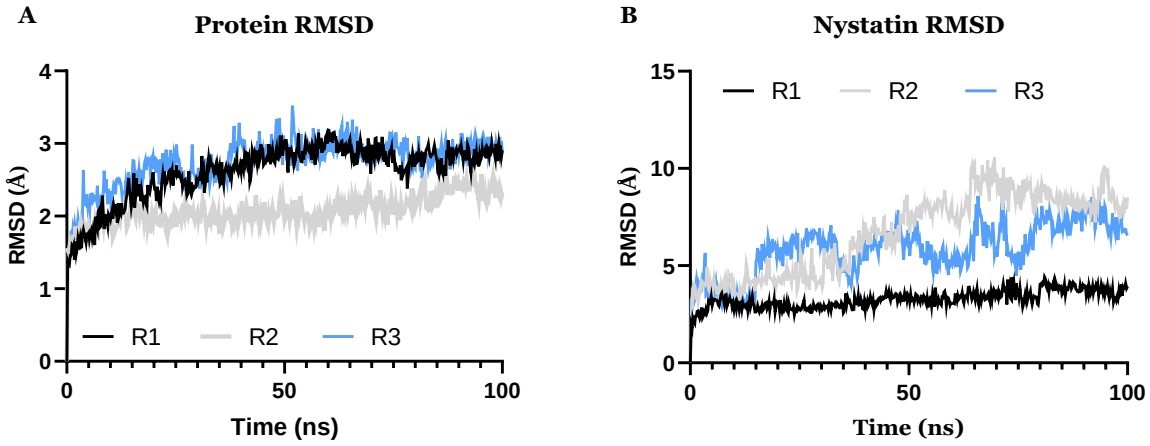

Figure S7. Representative picture of root mean square deviation (RMSD) values of protein backbone for the RdRp complexes (**A**); Ligand RMSD variation along the simulation time for nystatin (**B**).

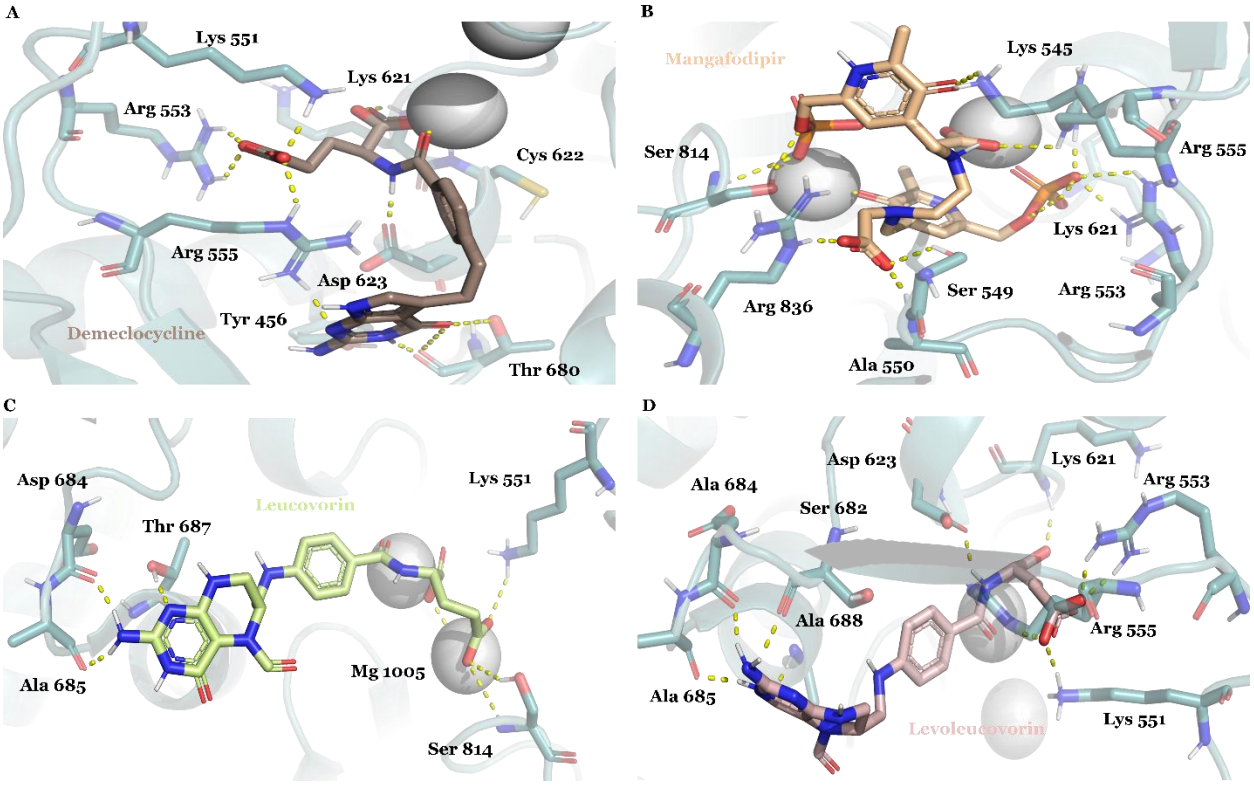

Figure S8. Representative snapshot of the docking poses best ranked compounds in RdRp. RdRp's residues are colored according to the atom type of the interacting amino-acid residues (protein's carbon, light teal; oxygen, red; nitrogen, blue). The protein-ligand interactions are represented by dash lines as follow: hydrogen bond interactions are colored in yellow; π-π interactions are colored in blue.

References

1. Jin, Z.; Du, X.; Xu, Y.; Deng, Y.; Liu, M.; Zhao, Y.; Zhang, B.; Li, X.; Zhang, L.; Peng, C.; et al. Structure of M from SARS-CoV-2 and Discovery of Its Inhibitors. *Nature* **2020**, *582*, 289–293.
2. Kim, S.H.; MacIntyre, D.A.; Hanyaloglu, A.C.; Blanks, A.M.; Thornton, S.; Bennett, P.R.; Terzidou, V. The Oxytocin Receptor Antagonist, Atosiban, Activates pro-Inflammatory Pathways in Human Amnion via G(αi) Signalling. *Mol. Cell. Endocrinol.* **2016**, *420*, 11–23.
3. Pandey, P.; Khan, F. A Mechanistic Review of the Anticancer Potential of Hesperidin, a Natural Flavonoid from Citrus Fruits. *Nutr. Res.* **2021**, *92*, 21–31.
4. Radu, D.; Åhlin, A.; Svanborg, P.; Lindefors, N. Anxiogenic Effects of the CCK B Agonist Pentagastrin in Humans and Dose-Dependent Increase in Plasma C-Peptide Levels. *Psychopharmacology* **2002**, *161*, 396–403.
5. Aggerbeck, M.; Guellaën, G.; Hanoune, J. N-Aralkyl Substitution Increases the Affinity of Adrenergic Drugs for the Alpha-Adrenoceptor in Rat Liver. *Br. J. Pharmacol.* **1979**, *65*, 155–159.

6. Ackerson, N.O.B.; Liberatore, H.K.; Plewa, M.J.; Richardson, S.D.; Ternes, T.A.; Duirk, S.E. Disinfection Byproducts and Halogen-Specific Total Organic Halogen Speciation in Chlorinated Source Waters–The Impact of Iopamidol and Bromide. *J. Environ. Sci.* **2020**, *89*, 90–101.
7. Meijenhorst, G.C.; de Bruin, J.N. Hexabrix (ioxaglate), a New Low Osmolality Contrast Agent for Lumbar Epidural Double-Catheter Venography. *Neuroradiology* **1980**, *20*, 29–32.
8. Garriga, C.; Pérez-Elías, M.J.; Delgado, R.; Ruiz, L.; Nájera, R.; Pumarola, T.; del Mar Alonso-Socas, M.; García-Bujalance, S.; Menéndez-Arias, L. Mutational Patterns and Correlated Amino Acid Substitutions in the HIV-1 Protease after Virological Failure to Nelfinavir- and Lopinavir/ritonavir-Based Treatments. *J. Med. Virol.* **2007**, *79*, 1617–1628.
9. Karlgren, M.; Vildhede, A.; Norinder, U.; Wisniewski, J.R.; Kimoto, E.; Lai, Y.; Haglund, U.; Artursson, P. Classification of Inhibitors of Hepatic Organic Anion Transporting Polypeptides (OATPs): Influence of Protein Expression on Drug–Drug Interactions. *J. Med. Chem.* **2012**, *55*, 4740–4763.
10. Zwiener, C.; Glauner, T.; Sturm, J.; Wörner, M.; Frimmel, F.H. Electrochemical Reduction of the Iodinated Contrast Medium Iomeprol: Iodine Mass Balance and Identification of Transformation Products. *Anal. Bioanal. Chem.* **2009**, *395*, 1885–1892.
11. Chow, S.L.; Ng, T.M.H.; Litwinski, R.A.; Kangavari, S.; Weiss, M. Effect of Iodixanol and Ioxilan on QT Interval and Renal Function in Patients with Systolic Heart Failure. *Int. J. Cardiol.* **2012**, *154*, 17–21.
12. Diaz-Montero, C.M.; Wang, Y.; Shao, L.; Feng, W.; Zidan, A.-A.; Pazoles, C.J.; Montero, A.J.; Zhou, D. The Glutathione Disulfide Mimetic NOV-002 Inhibits Cyclophosphamide-Induced Hematopoietic and Immune Suppression by Reducing Oxidative Stress. *Free Radic. Biol. Med.* **2012**, *52*, 1560–1568.
13. Stover, P.J.; Field, M.S. Trafficking of Intracellular Folates. *Adv. Nutr.* **2011**, *2*, 325–331.
14. Chuang, V.T.G.; Suno, M. Levoleucovorin as Replacement for Leucovorin in Cancer Treatment. *Ann. Pharmacother.* **2012**, *46*, 1349–1357.
15. Adolph, J.M.G.; Engelkamp, H.; Herbig, W.; Peters, P.E.; Wenzel-Hora, B.I. Iotrolan in Urography: Efficacy and Tolerance in Comparison with Iohexol and Iopamidol. *Eur. Radiol.* **1995**, *5*, S63–S68.
16. Gan, X.-D.; Wei, B.-Z.; Fang, D.; Fang, Q.; Li, K.-Y.; Ding, S.-L.-Y.; Peng, S.; Wan, J. Efficacy and Safety Analysis of New P2Y12 Inhibitors versus Clopidogrel in Patients with Percutaneous Coronary Intervention: A Meta-Analysis. *Curr. Med. Res. Opin.* **2015**, *31*, 2313–2323.
17. Holleran, J.L.; Parise, R.A.; Guo, J.; Kiesel, B.F.; Taylor, S.E.; Percy Ivy, S.; Chu, E.; Beumer, J.H. Quantitation of Iohexol, a Glomerular Filtration Marker, in Human Plasma by LC–MS/MS. *J. Pharm. Biomed. Anal.* **2020**, *189*, 113464.
18. Dhondt, L.; Croubels, S.; De Cock, P.; Dhont, E.; De Baere, S.; De Paepe, P.; Devreese, M. Volumetric Absorptive Microsampling as Alternative Sampling Technique for Renal Function Assessment in the Paediatric Population Using Iohexol. *J. Chromatogr. B Anal. Technol. Biomed. Life Sci.* **2021**, *1171*, 122623.

19. Hofmann, M.; Maecke, H.; Börner, A.; Weckesser, E.; Schöffski, P.; Oei, M.; Schumacher, J.; Henze, M.; Heppeler, A.; Meyer, G.; et al. Biokinetics and Imaging with the Somatostatin Receptor PET Radioligand 68Ga-DOTATOC: Preliminary Data. *Eur. J. Nucl. Med.* **2001**, *28*, 1751–1757.
20. Carlquist, M.; Frejd, T.; Gorwa-Grauslund, M.F. Flavonoids as Inhibitors of Human Carbonyl Reductase 1. *Chem. Biol. Interact.* **2008**, *174*, 98–108.
21. Zoghbi, G.J.; Iskandrian, A.E. Selective Adenosine Agonists and Myocardial Perfusion Imaging. *J. Nucl. Cardiol.* **2012**, *19*, 126–141.
22. Hirshfeld, J.W., Jr.; Wieland, J.; Davis, C.A.; Giles, B.D.; Passione, D.; Ray, M.B.; Ripley, N.S. Hemodynamic and Electrocardiographic Effects of Ioversol during Cardiac Angiography. Comparison with Iopamidol and Diatrizoate. *Investig. Radiol.* **1989**, *24*, 138–144.
23. Grossman, R.I.; Modic, M.T. A Randomized Comparison of Iodixanol and Iohexol in Adult Intracranial Computed Tomography Scanning. *Acad. Radiol.* **1996**, *3* (Suppl. 3), S488–S494.
24. Saif, M.W.; Parikh, R.; Ray, D.; Kaye, J.A.; Kurosky, S.K.; Thomas, K.; Ramirez, R.A.; Halfdanarson, T.R.; Beveridge, T.J.R.; Mirakhur, B.; et al. Medical Record Review of Transition to Lanreotide Following Octreotide for Neuroendocrine Tumors. *J. Gastrointest. Oncol.* **2019**, *10*, 674–687.
25. Peters, F.; Ellermann, I.; Steinbicker, A.U. Intravenous Iron for Treatment of Anemia in the 3 Perisurgical Phases: A Review and Analysis of the Current Literature. *Anesth. Analg.* **2018**, *126*, 1268–1282.
26. Geisser, P.; Burckhardt, S. The Pharmacokinetics and Pharmacodynamics of Iron Preparations. *Pharmaceutics* **2011**, *3*, 12–33.
27. Charytan, C.; Levin, N.; Al-Saloum, M.; Hafeez, T.; Gagnon, S.; Van Wyck, D.B. Efficacy and Safety of Iron Sucrose for Iron Deficiency in Patients with Dialysis-Associated Anemia: North American Clinical Trial. *Am. J. Kidney Dis.* **2001**, *37*, 300–307.
28. R, L.; A, Y.; J, M.; L, F.; V, J. The Affect of Goserelin on the QoL of Women Having Chemotherapy for EBC: Results from the OPTION Trial. *Breast* **2020**, *52*, 122–131.
29. Aljabri, B.; Lilleby, W.; Switlyk, M.D.; Tafjord, G. Restart of Androgen Deprivation Therapy after Goserelin Induced Pituitary Apoplexy in a Patient with Disseminated Prostate Cancer a Case Report and Five-Years Follow-Up. *Urol. Case Rep.* **2021**, *37*, 101648.
30. Tuyen, D.T.; Yew, G.Y.; Cuong, N.T.; Hoang, L.T.; Yen, H.T.; Thao, P.T.H.; Thao, N.T.; le Thanh, N.S.; Trang, N.T.H.; Trung, N.T.; et al. Selection, Purification, and Evaluation of Acarbose–an α-Glucosidase Inhibitor from Actinoplanes Sp. *Chemosphere* **2021**, *265*, 129167.
31. Wang, Z.; Wang, J.; Hu, J.; Chen, Y.; Dong, B.; Wang, Y. A Comparative Study of Acarbose, Vildagliptin and Saxagliptin Intended for Better Efficacy and Safety on Type 2 Diabetes Mellitus Treatment. *Life Sci.* **2021**, *274*, 119069.
32. Loho, T.; Dharmayanti, A. Colistin: An Antibiotic and Its Role in Multiresistant Gram-Negative Infections. *Acta Med. Indones.* **2015**, *47*, 157–168.
33. Weiner, C.P.; Buhimschi, C. *Drugs for Pregnant and Lactating Women E-Book*; Elsevier Health Sciences: Hoboken, NJ, USA, 2009; ISBN 9781437721362.
34. Barza, M. Imipenem: First of a New Class of Beta-Lactam Antibiotics. *Ann. Intern. Med.* **1985**, *103*, 552–560.

35. Deeks, E.D.; Perry, C.M. Zoledronic Acid. *Drugs Aging* **2008**, *25*, 963–986.
36. Wellington, K.; Goa, K.L. Zoledronic Acid. *Drugs* **2012**, *63*, 417–437.
37. Zhong, X.; Ma, Z.; Su, Y.; Li, Z.; Liao, Y.; Pan, X.; Zang, L.; Zhou, S. Flavin Adenine Dinucleotide Ameliorates Hypertensive Vascular Remodeling via Activating Short Chain Acyl-CoA Dehydrogenase. *Life Sci.* **2020**, *258*, 118156.
38. Chung, B.H.; Horie, S.; Chiong, E. Clinical Studies Investigating the Use of Leuprorelin for Prostate Cancer in Asia. *Prostate Int.* **2020**, *8*, 1–9.
39. Bhowmick, N.A.; Oft, J.; Dorff, T.; Pal, S.; Agarwal, N.; Figlin, R.A.; Posadas, E.M.; Freedland, S.J.; Gong, J. COVID-19 and Androgen-Targeted Therapy for Prostate Cancer Patients. *Endocr. Relat. Cancer* **2020**, *27*, R281–R292.
40. Müller, J.; Jewell, K.S.; Schulz, M.; Hermes, N.; Ternes, T.A.; Drewes, J.E.; Hübner, U. Capturing the Oxic Transformation of Iopromide–A Useful Tool for an Improved Characterization of Predominant Redox Conditions and the Removal of Trace Organic Compounds in Biofiltration Systems? *Water Res.* **2019**, *152*, 274–284.